



A simplified coupled crankshaft–engine block model



Bilel Bellakhdhar^{a,*}, Abdelwaheb Dogui^a, Jean-Louis Ligier^b

^a Laboratory of Mechanical Engineering, National Engineering School of Monastir, University of Monastir, Avenue Ibn Eljazzar, 5019 Monastir, Tunisia

^b Haute École d'ingénierie et de gestion du canton de Vaud (HEIG-VD), 1, route de Cheseaux, CH-1400 Yverdon-les-Bains, Switzerland

ARTICLE INFO

Article history:

Received 19 December 2011

Accepted 28 September 2013

Available online 22 October 2013

Keywords:

Bearing loads

Crankshaft

Stiffness

Beam model

Deformation

Misalignment

ABSTRACT

Modern highly loaded crankshafts and bearing improvement requires an accurate knowledge of the acting forces. This information is now provided by quick and robust design tools based on simplified coupled engine block–crankshaft models. In this paper, a model based on beam theory is proposed. Several considerations are addressed. Among these considerations are bearing misalignments, crankshaft bending stiffness, clearance, hydrodynamic sustentation and bearing deformation stiffness. The model substitutes efficiently engine simulation in crankshaft and bearing preliminary design.

© 2013 Académie des sciences. Published by Elsevier Masson SAS. All rights reserved.

1. Introduction

Suitable choice of the crankshaft and bearing dimensions must be made in the early phase of the engine design process. This choice requires several design iterations. In such a situation, it is not easy to have resorts to structural finite elements analysis, which requires important means of calculation and a lot of time. To be competitive, it is required to develop a fast and accurate engine system model coupling crankshaft and main bearing structural models by hydrodynamic assessment.

Many kinds of crankshaft–bearing model have been reported in the past. At an early stage, a statically determinate scheme was used [1–4]. The loads carried by each throw are not distributed across all of bearings, which is a rough approximation. After that, a statically indeterminate scheme was considered [2,5]. Crankshaft is assumed to continuous beam resting on rigid supports. This approximation is closer to real conditions [5–7]. Afterwards, the main bearing was modelled by non-linear springs [6]. Then, a coupled quasi-static crank model and a hydrodynamic bearing model were defined [8,9]. Recently, a coupled crankshaft–block dynamics model through hydrodynamics was established [10,11]. But these sophisticated models require a lot of information and important calculation resources. So, the classical analysis methods remain attractive and they are still used in the concept design phase to support the choice of the crankshaft and of the bearing dimensions [13,14]. These analyses use simple approaches and give quick and sufficiently accurate results.

In this paper, a quasi-static engine system model based on beam theory is represented. The crankshaft of a four-cylinder engine is modelled by a cylindrical continuous beam, composed of four sections with elliptic cross-sections and based on five supports. The governing equations system relating bearing reactions to supports motions is established. The crankshaft elasticity is considered in the equation system through the four throw inertia moments. The behavior of the main bearing which is the major non-linear component in the system is investigated. A new main bearing behavior law is suggested. This

* Corresponding author. Tel.: +216 97 775 038.

E-mail addresses: bileling@yahoo.fr (B. Bellakhdhar), abdel.dogui@enim.rnu.tn (A. Dogui), jean-louis.ligier@heig-vd.ch (J.-L. Ligier).

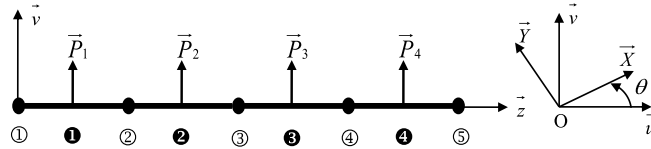


Fig. 1. Beam model.

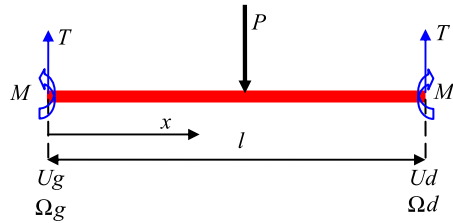


Fig. 2. Throw between two main bearings.

behavior law takes into account, in the same time, the clearance, the hydrodynamic assessment and the bearing deformation stiffness. The model carried out is used to calculate the main bearing loads.

2. Modeling of crankshaft system

In quasi-static engine models, the crankshaft can be modelled in different ways. It is often assumed as a beam [15] or as an assembly of beam finite elements [16]. Sometimes; it is modelled as a system of rigid elements connected with flexion springs [6]. In this work, the crankshaft is assumed as a continuous beam composed of four sections (one for each throw) with elliptic cross-sections, resting on five supports simulating the main bearings. With each support i are associated the following vectors: a reaction force \underline{R}_i , a reaction moment \underline{M}_i , a displacement \underline{U}_i (of the “crankshaft beam” at the mid-bearing position), a rotation $\underline{\Omega}_i$ (of the beam cross-section at the mid-bearing position), a misalignment \underline{d}_i (which define the locus of the bearing centre relative to a common straight reference line to all the supports) and a clearance \underline{J}_i (the clearance is supposed to be elliptic).

All the vectors defined above are represented as horizontal and vertical components in their planes perpendicular to the crankshaft axis. Each throw of length l_i has two flexion inertia J_{Xi} and J_{Yi} to take into account the crankshaft elasticity and it is loaded by a concentrated connecting rod load $\underline{P}_i(\theta)$. The X and Y axes are the principal inertia axes (Fig. 1).

This deviated bending problem is decomposed into two pure bending problems in the two symmetry planes of the beam (\vec{X}, \vec{Z}) and (\vec{Y}, \vec{z}) .

Considering a throw between two bearings in the (\vec{X}, \vec{z}) plane (Fig. 2). We denote by:

- T and M the shear and the bending moment at the left extremity, respectively;
- T' and M' the shear and the bending moment at the right extremity, respectively;
- U_l and U_r the left-side and the right-side displacements, respectively;
- Ω_l and Ω_r the left-side and the right-side cross-section rotation, respectively;
- E the Young modulus.

The static equilibrium allows the determination of T' and M' .

The bending moment along the section is piecewise linear with respect to z . Therefore, the cross-section rotation is quadratic with respect to z and the displacement is cubic with respect to z .

The boundary conditions below allow the determination of the cross-section rotation $\Omega(z)$ and of the beam displacement $U(z)$ along the beam:

$$\Omega(0) = \Omega_l; \quad \Omega(l) = \Omega_r; \quad U(0) = U_l; \quad U(l) = U_r$$

The continuity of displacement and rotation at $z=l/2$ generates the following two equations:

$$\Omega_l = \frac{U_r - U_l}{l} - \frac{(8T + P)l^2 - 24lM}{48E J_X} \tag{1a}$$

$$\Omega_r = \frac{U_r - U_l}{l} + \frac{(16T + 5P)l^2 - 24lM}{48E J_X} \tag{1b}$$

Replacing M with $-M$ and J_X by J_Y leads to the same previous relations in the (\vec{Y}, \vec{z}) plane.

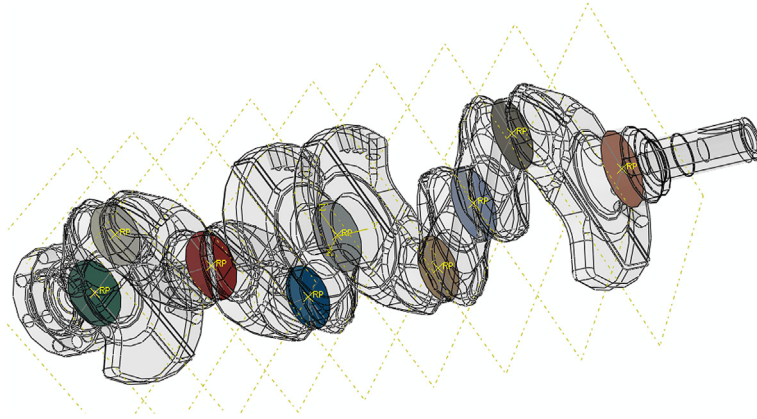


Fig. 3. Crankshaft.

The equilibrium equation added to the four equations (one for each throw) gives a linear system with five equations for each bending plane (Eq. (2)), connecting reaction forces to displacements at mid-bearing positions.

$$\underline{A}_X \underline{R}_X + \underline{B}_X \underline{U}_X + \underline{C}_X \underline{P}_X = 0 \tag{2a}$$

$$\underline{A}_Y \underline{R}_Y + \underline{B}_Y \underline{U}_Y + \underline{C}_Y \underline{P}_Y = 0 \tag{2b}$$

\underline{R}_X , \underline{R}_Y , \underline{U}_X and \underline{U}_Y are 1-by-5 matrices. \underline{P}_X and \underline{P}_Y are a 1-by-4 matrices. \underline{A}_X , \underline{A}_Y , \underline{B}_X and \underline{B}_Y are square matrices (5-by-5). \underline{C}_X and \underline{C}_Y are 5-by-4 matrices (Appendix A).

These equations are established in the rotating coordinate system $\mathcal{R}(X, Y, z)$ attached to the crankshaft. Expressing these equations in the fixed coordinate system $\mathcal{R}_o(u, v, z)$ attached to the engine block, we obtain a 10-equation linear system:

$$\underline{A} \underline{R} + \underline{B} \underline{U} + \underline{C} \underline{P} = 0 \tag{3}$$

To solve this system, we need to know the crankshaft elasticity (represented by the cross-sections inertias J_X and J_Y) and the bearing stiffness.

3. The crankshaft bending stiffness

The crankshaft elasticity is usually considered to be constant over the length of the shaft. This is, of course, a rough approximation. The traditional bending stiffness determination method consists in carrying out a “three-point” bending test on the real crankshaft [6,8]: the crankshaft is resting on two V supports at the extreme mid-bearing positions. The bending effort is applied at the central pivot middle. The average stiffness is then obtained through a traditional bi-supported beam model by the ratio of the applied force to the deflection measured at the force application point. The test conditions are very different from the real operating conditions of the crankshaft. So the calculated stiffness is not accurate [12], which affects the bearings load distribution.

A new methodology based on a finite elements model using the crankshaft real CAD was established [12]. The real crankpins loads along the driving cycle are applied at mid-pins cross positions for different angular positions of the crankshaft. In order to approach the beam model with the rigid supports defined previously, the mid-bearings cross-sections’ centres are blocked in translation movements in the plane perpendicular to the crankshaft axis. See Fig. 3.

For each crankshaft position, the bearings loads (at bearings reference points) and deflections in the mid-pins positions (the mid-pins reference point’s motion) are calculated. Scaling (adjusting) finite elements results to beam model results, the flexion inertias J_{Xi} and J_{Yi} of each throw are identified. So, the cross-sections geometrical characteristics of the crankshaft beam are identified.

4. The main bearing behavior law

The crankshaft model, as described in the previous paragraphs, is supported at the main bearing locations. The supports are modelled by concentrated stiffness at the mid-bearings positions. The bearing loads consist only of reaction forces. The main objective of this paragraph is to establish a bearing behavior law for use in the beam model. This behavior law connects the bearing reaction to the beam motion compared to the housing centre. This reaction force appears when the crankshaft beam crushes the main bearing through hydrodynamic lubrication. Thus the main bearing stiffness depends on various parameters:

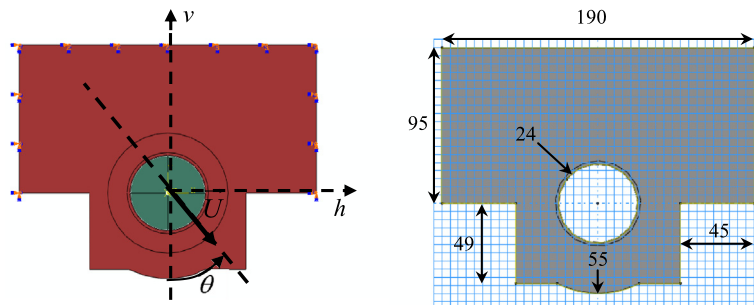


Fig. 4. Finite element model.

- the radial clearance of the bearing,
- the hydrodynamic assessment stiffness,
- the main bearing deformation stiffness.

The two first aspects are investigated through analytic and finite element models [16]. The major findings are:

- the clearance influences the bearing stiffness, especially under the action of low loadings.
- the oil film has a very low stiffness for low loads and becomes very rigid for important loadings.

The deformation stiffness is investigated below through an appropriate finite-element model.

4.1. Finite-element model of a bearing

The finite-element model of the main bearing is shown in Fig. 4 and is composed of two parts. The first part includes the bearing liners, the main bearing cap, and the top half of the main bearing housing supposed to be interdependent. The bearing liners are composed of two layers: aluminum (Young's modulus $E = 70$ GPa, Poisson's ratio $\nu = 0.33$) inner layer of 0.3 mm of thickness, and steel ($E = 210$ GPa, $\nu = 0.3$) external layer of 1.7 mm of thickness. The second part is the shaft made of steel. It has a rigid central portion of radius 1 mm. The considered clearance in the bearing is about 30 μm . The thickness of the main bearing is 22 mm. The contact is supposed to be frictionless.

The model of the main bearing consists of 13 105 nodes and 12 834 elements (four-node bilinear plane strain quadrilateral with reduced integration elements CPE4R and three-node linear plane strain triangle elements CPE3).

The nodes on the side and top surfaces of the main bearing housing are assumed fixed. A displacement U is imposed to the reference point of the rigid part of the shaft. So the shaft crushes the bearing liner and we obtain a reaction force.

The bearing deformation was usually thought to be caused only by the cylinder block elasticity. However, the first finding is that the shaft deformation is not negligible. The displacement isovalues of Fig. 5(a) affirm that.

The curve in Fig. 5(b) shows the proportion of the displacement of the shaft center compared to the housing center due to the shaft deformation and according to the loading direction θ . The proportion of the shaft deformation reaches 44% of the overall deformation.

4.2. Deformation stiffness submodel

Knowing that the clearance effect occurs for low loads, the deformation stiffness is assimilated to the slope of linear portion of the shaft motion/reaction force curve (corresponding to high loads, Fig. 6(a)).

The curves in Fig. 6(b) show the evolution of the deformation stiffness K_d according to the loading orientation θ in the case of a rigid shaft and a deformable shaft.

The housing deformation stiffness varies considerably. The stiff shaft gives a low vertical deformation stiffness ($\theta = 0^\circ$), which is 26% more than that given by deformable shaft and a high vertical deformation stiffness ($\theta = 180^\circ$), which is 69% more than that given deformable shaft.

The shape of the deformation stiffness curve is like that of a sigmoid. It is thus proposed to model this curve by the following function:

$$K_d(\theta) = k_{lv} + \frac{k_{hv} - k_{lv}}{1 + \exp\left(\frac{\theta_0 - \theta}{\Delta\theta}\right)} \quad (4)$$

where:

- k_{lv} is the low vertical deformation stiffness,
- k_{hv} is the high vertical deformation stiffness,

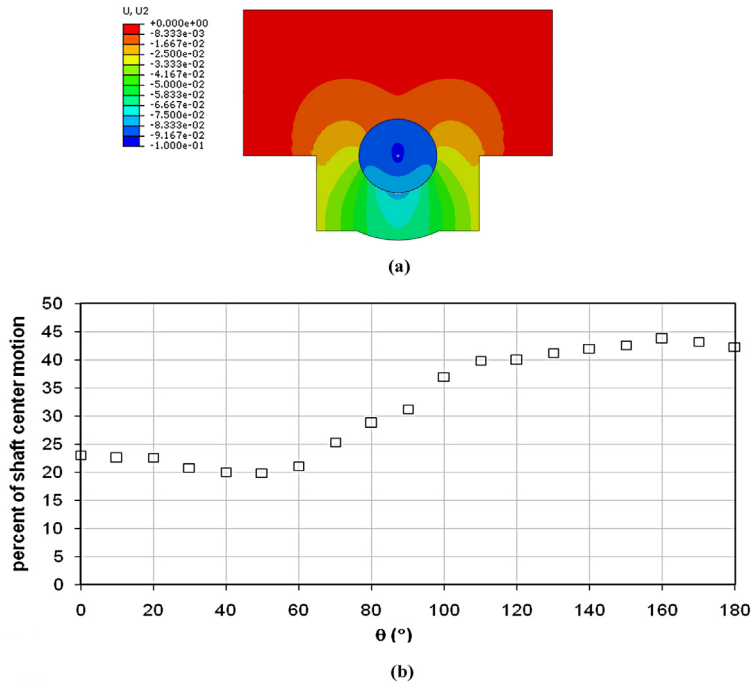


Fig. 5. Shaft deformation.

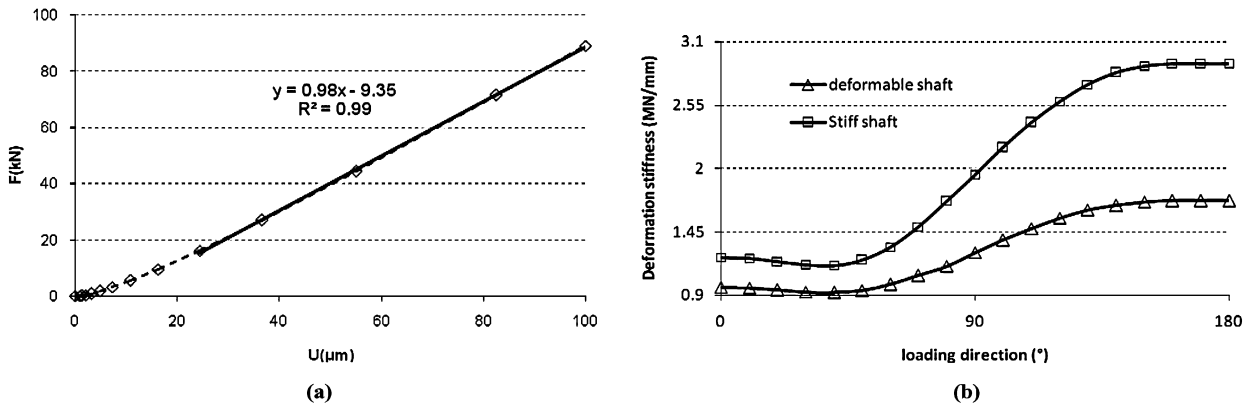


Fig. 6. (a) Deformation stiffness determination. (b) Deformation stiffness evolution.

θ is the loading direction,

θ_0 is a parameter that defines the abscissa of the concavity of the curve,

$\Delta\theta$ is a parameter that permits to modify the curve central slope.

The parameters values identified from the finite-element curves for the stiff shaft and the deformable shaft are very close. θ_0 is about 97° and $\Delta\theta$ is about 15° . The quality of identification is shown in Fig. 7.

The sigmoid model represents well the deformation stiffness curve.

4.3. Overall bearing stiffness model

For a given bearing load R^b applied to the shaft, his displacement U^b is the sum of hydrodynamic displacement U_h^b obtained by the hydrodynamic lubrication model and elastic displacement due to the structure deformation U_d^b .

In order to make calculations close to real conditions, the bearing of a four-cylinder internal combustion diesel engine was considered. The hydrodynamic bearing theory is used for the oil film deformation calculation [17]. Table 1 shows the configuration parameters of the bearing. Fig. 8 shows the effort curves:

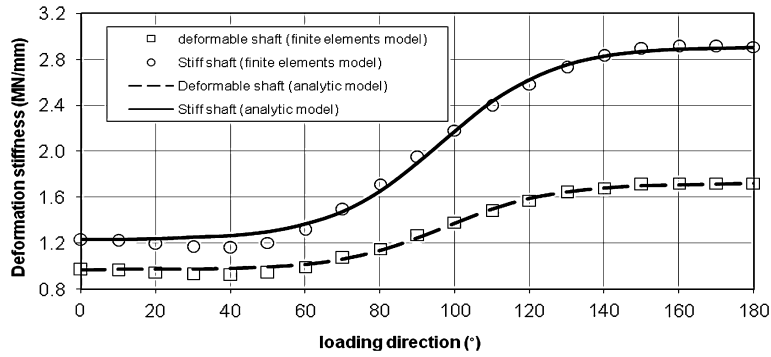


Fig. 7. Stiffness circumferential variation.

Table 1

Configuration parameters of crankshaft bearing.

Radius of the main bearing (mm)	24
Bearing clearance (μm)	30
Bearing width (mm)	22
Oil viscosity μ (ns/m ²)	0.005
Crankshaft full rotation speed (rpm)	4000

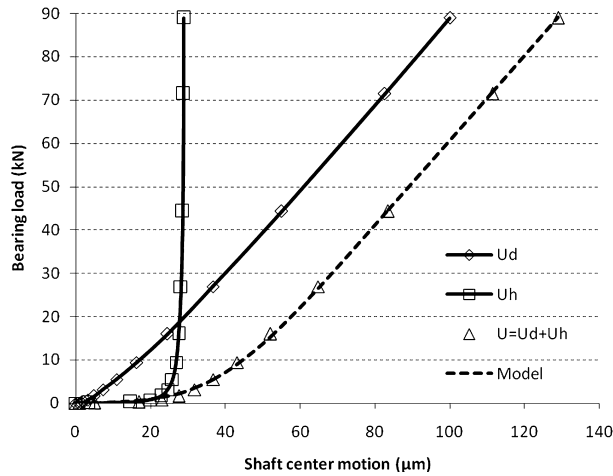


Fig. 8. Shaft motion/bearing load curves.

- $R^b(U_d^b)$ corresponding to the bearing load versus the shaft centre displacement due to elastic deformation,
- $R^b(U_h^b)$ corresponding to the bearing load versus the shaft centre displacement due to oil film deformation,
- $R^b(U^b = U_h^b + U_d^b)$ corresponding to the bearing effort versus the total shaft centre displacement.

We propose the regularization of the stiffness function $K = dR^b/dU^b$ according to the following model:

$$K(U^b) = K_d \left[1 - \frac{1 + e^{-\frac{J}{dx}}}{1 + e^{-\frac{U^b - J}{dx}}} \right] \tag{5}$$

where K_d is the deformation stiffness, J is the clearance parameter and dx is the regularization parameter.

The integration of the stiffness function $K(U^b)$ gives the following bearing load model:

$$R^b(U^b) = K_d \left[dx(1 + e^{-\frac{J}{dx}}) \ln \left(\frac{1 + e^{-\frac{U^b - J}{dx}}}{1 + e^{-\frac{J}{dx}}} \right) - U^b e^{-\frac{J}{dx}} \right] \tag{6}$$

This bearing load model is identified starting from the curve $R^b(U^b = U_h^b + U_d^b)$ of Fig. 8. The identified values of the model parameters are $dx = 9.65 \mu\text{m}$ and $J = 37 \mu\text{m}$. The quality of the model is shown in the dotted-line curve of Fig. 8.

The model ensures properly the transition from the low-rigidity configuration to the high-rigidity configuration.

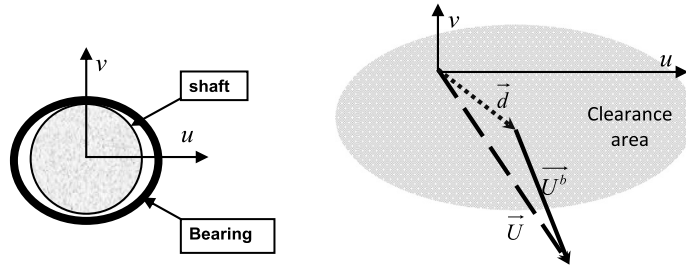


Fig. 9. Modeling of the bearing.

Replacing the deformation stiffness K_d with the submodel defined in Section 4.2, we end up with a main bearing behavior law that combines clearance effect, hydrodynamic sustentation and deformation stiffness:

$$R(U, \theta) = \left[k_{lv} + \frac{k_{hiv} - k_{lv}}{1 + \exp\left(\frac{\theta_0 - \theta}{\Delta\theta}\right)} \right] \left[dx(1 + e^{-\frac{J}{dx}}) \ln\left(\frac{1 + e^{\frac{U-J}{dx}}}{1 + e^{-\frac{J}{dx}}}\right) - Ue^{-\frac{J}{dx}} \right] \quad (7)$$

Moreover, this behavior law takes into account the circumferential variation of the deformation stiffness.

The merit of the proposed bearing behavior law is that it can be advantageously useful in beam crankshaft–engine block combined models.

5. Formulation of the crankshaft–engine block model

The crankshaft model is described in the fixed engine block system by Eq. (3).

The vector \underline{U} defines the center shaft position relative to the straight common bearings line. \underline{U} is the sum of the vector \underline{U}^b that defines the center shaft position relative to the bearing center and the misalignment vector \underline{d} (Fig. 9).

Eq. (3) can be written as:

$$\underline{AK}(\underline{U}^b)\underline{U}^b + \underline{B}(\underline{U}^b + \underline{d}) + \underline{C}P = \underline{0} \quad (8)$$

where \underline{K} is the block diagonal stiffness matrix. (K_1, K_2, K_3, K_4, K_5) are the eigenvalues (the principal rigidities):

$$K_i(U_i^b, \theta_i) = \left[k_{ilv} + \frac{k_{ihv} - k_{ilv}}{1 + \exp\left(\frac{\theta_0 - \theta_i}{\Delta\theta}\right)} \right] \left[1 - \frac{1 + e^{-\frac{J}{dx}}}{1 + e^{\frac{U_i^b - J}{dx}}} \right] \quad (9)$$

k_{ilv} and k_{ihv} are respectively the low vertical and the high vertical deformation stiffness of the bearing number i .

The equation system (8) characterizes the static equilibrium of the crankshaft on five elastic and misaligned bearings. Because of the non-linearity, the system is resolved using an iterative process.

The finding of the solution is conducted in an iterative way from an initial value of displacements in the bearings.

6. Selected results and discussion

6.1. Validation of the suggested model

In this section, the accuracy and efficiency of the developed coupled crankshaft–engine block model is demonstrated by comparison with an elastohydrodynamic calculation with AVL-EXCITE software.

The studied engine is a four-cylinder in line engine. The main bearings are supposed to be similar. The distance between two bearings is about 85 mm. The bearing characteristics are illustrated in Table 1. The low vertical stiffness is about 0.98×10^9 N/m and the high vertical stiffness is about 1.72×10^9 N/m.

The values of the bearing stiffness model parameters are those identified previously in paragraph 3 ($dx = 9.65 \mu\text{m}$ and $J = 37 \mu\text{m}$).

All bearings are supposed to be perfectly aligned. So the misalignment vector \underline{d} is null.

The considered crankshaft bending rigidities are presented in Table 2.


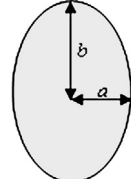
The real loading corresponding to a four-cylinder in-line engine is applied. The engine operating conditions are 4000 rpm and full load. Loading is periodic and in phase with the combustion cycle of the engine. Fig. 10 shows the time history of the horizontal and vertical loads applied to the crankpin 1 along the driving cycle.

The real loads are applied at mid-pins cross positions for different angular positions of the crankshaft.

The duration of a complete simulation along the entire engine cycle is about 20 s. The simulation is done for each degree of the crank angle.

Table 2
Crankshaft inertias [12]

	J_X (mm ⁴)	J_Y (mm ⁴)	a (mm)	b (mm)
Throw 1	49468	53971	15.67	16.37
Throw 2	55768	53634	16.40	16.09
Throw 3	55768	53634	16.40	16.09
Throw 4	49468	53971	15.67	16.37

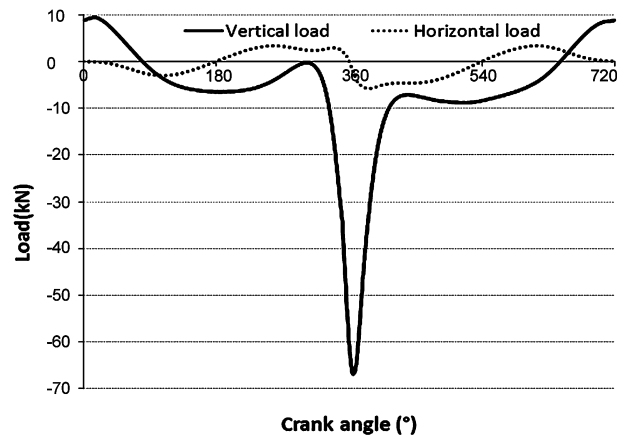


Fig. 10. Loads applied to a crankpin.

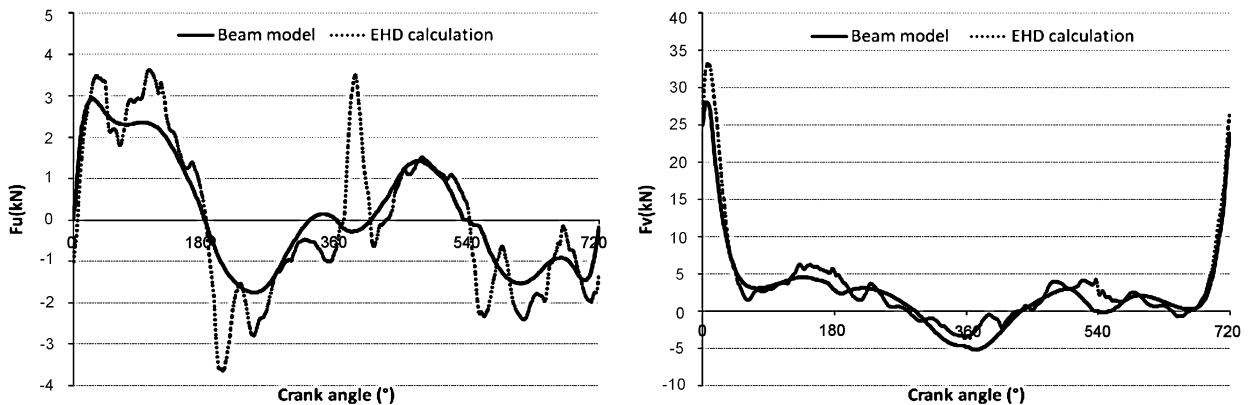


Fig. 11. Forces in main bearing-1.

Figs. 11–13 show the horizontal component “ F_u ” and the vertical component “ F_v ” of the main bearing loads calculated using the suggested model and the elastohydrodynamic calculation. For consideration of symmetry, only main bearing-1, -2 and -3 are presented. The horizontal axis represents the crank angle in a thermodynamic cycle. Zero degrees correspond to cylinder one firing TDC. The engine firing order is 1–3–4–2.

Fig. 11 shows the results for bearing-1. The suggested model is in a good agreement with the elastohydrodynamic model along the majority of the driving cycle. It underestimates the maximum vertical load of about 15%.

Bearing-1 load is almost exclusively affected by the combustion of cylinder 1. The other cylinder combustions are detected by the suggested model by a vertical load decrease at 180°, 360°, and 540°.

Bearing-2 results show that the two calculations are in a good agreement for the vertical component along the majority of the driving cycle. It overestimates the maximum vertical load of about 9%. The horizontal components are different.

Bearing-3 load is affected by combustion in cylinders 1 and 2.

Fig. 13 shows the results for bearing-3. The two calculations are in a perfect agreement for both bearing loads components. Due to the middle position of the third bearing, the load is affected in a similar way by the combustion of cylinders 1 and 4 on the one hand and cylinders 2 and 3 on the other hand.

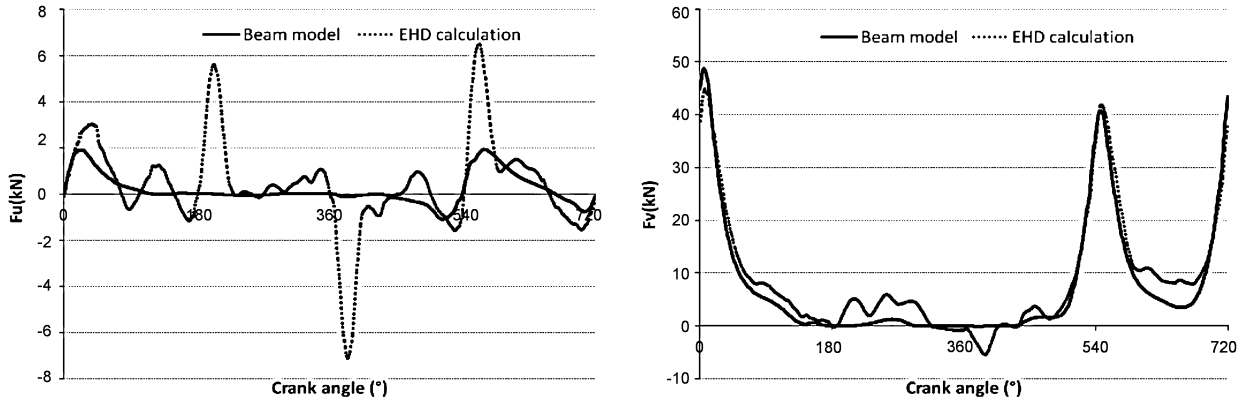


Fig. 12. Forces in main bearing-2.

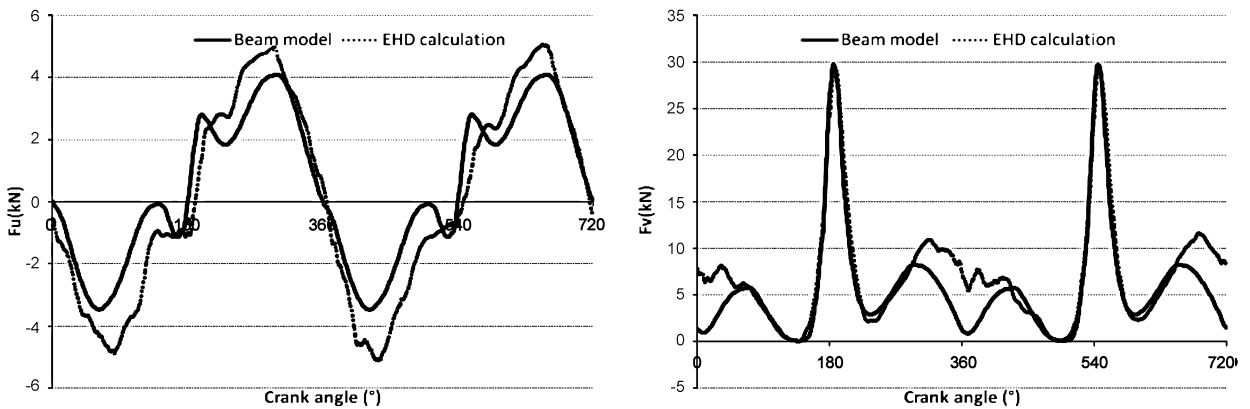


Fig. 13. Forces in main bearing-3.

Table 3
Misalignment effect on bearing loads.

	R1 max (N)	R2 max (N)	R3 max (N)
Max	29 876	52 351	34 825
Min	26 286	43 209	22 689
Average	27 944	48 518	29 385
% of bearing loads change	13%	19%	41%

The main bearing loads calculations are generally in a good agreement. Maximum main bearing loads are obtained at firing positions of the cylinders that are adjacent to the bearing. The greatest main bearing load occurs at bearing number two (about 48 kN).

The maximum main bearing load difference between the two models occurs for weak loads. However, this difference is not so important at firing positions.

6.2. Effect of the misalignments on the bearing loads

The crankshaft deformation is not only caused by the combustion loads transmitted to crankpins. It is also caused by the bearings misalignments resulting from manufacturing, assembly errors, cylinder block deformation, and thermal effects.

In this section, the misalignments are assumed to have only vertical components (*dvi*). The horizontal components (*dhi*) are considered null. The misalignment in each bearing varies from $-20 \mu\text{m}$ to $20 \mu\text{m}$ relatively to a straight reference line common to all the supports. A full factorial experimental design was applied to investigate the misalignment effect on the bearing loads. Its purpose is to determine which factors and factor interactions are statistically significant in affecting the bearing loads. Three levels of misalignment are considered for each bearing ($-20 \mu\text{m}$, $0 \mu\text{m}$, $20 \mu\text{m}$). Values of other parameters of the model are the same as considered previously.

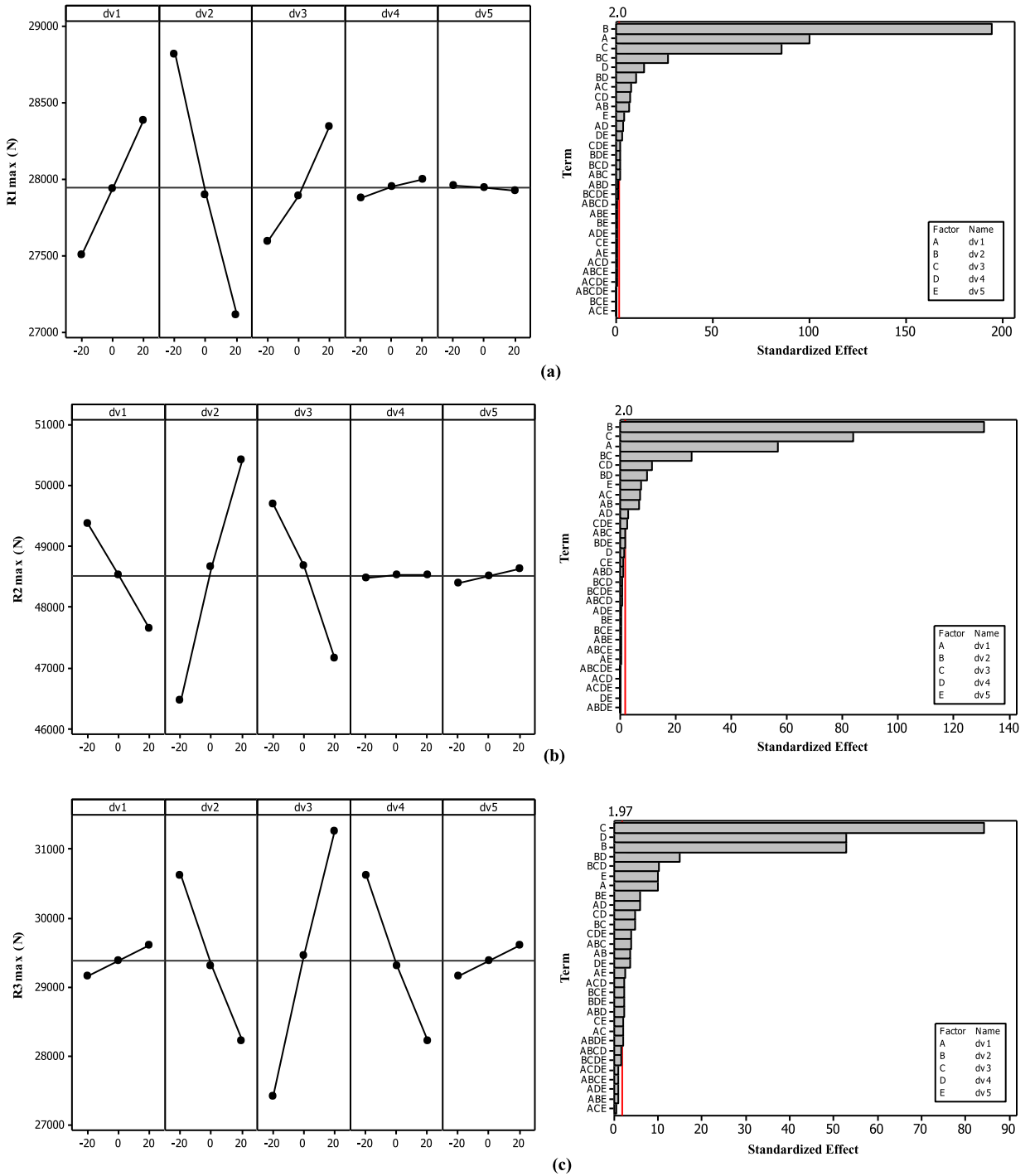


Fig. 14. The main effects and the Pareto plots of the bearing loads.

The data presented in Table 3 are the maximum, the average, and the minimum values of the maximum bearing loads along the driving cycle and the percentage of the maximum bearing loads change. These values are calculated from the numeric factorial experimental design described above.

As shown, misalignment affects considerably the bearing loads. It can cause 13% of variation of the maximum load of the bearing-1 maximum load, 19% of the bearing-2 maximum load, and 41% of the bearing-3 maximum load.

Numeric experimental design data are analyzed with MINITAB software. Figs. 14(a), (b), and (c) show respectively the main effect plots (on the left) and the Pareto plots (on the right) of bearings-1, -2, and -3.

The main effect plot illustrates means of factor levels and gives us information about the evolution of the response. The Pareto chart is performed to see which parameters are statistically significant.

Based on a 95% confidence interval, the misalignment of bearing-2 (dv2) has the most statistically significant impact on the maximum load of bearing-1, followed by dv1 and dv3, with almost the same effect. The most significant interaction is dv2 × dv3.

Furthermore, dv2 has the greatest effect on the maximum load of bearing-2, followed respectively by dv3, dv1, and the interaction dv2 × dv3.

Due to the middle position of bearing-3, its load is symmetrically affected; dv3 exerted the greatest effect on the maximum load, followed by dv2 and dv4, which present the same effect. The interactions dv2 × dv3 and dv2 × dv3 × dv4, and the parameters dv1 and dv5 had a much lower effect.

We conclude that all misalignments have significant effects on the bearings' behavior and thus on crankshaft loading. To design adequately the crankshaft and the main bearings, misalignment defects must be considered early in the design process as important parameters.

7. Conclusions

In this paper, a coupled crankshaft-bearings quasi-static beam model has been developed. The crankshaft is considered as an elastic continuous beam with elliptic cross-sections. A new bearing behavior law has been defined. This law connects the bearing reaction to the beam motion and it takes into consideration the anisotropic deformation stiffness, the clearance and the hydrodynamic assessment. The model loadings are the connecting rods loads and the bearings misalignments. The model may be used as a design support for the crankshaft and the associated components. The full simulation for an entire driving cycle is carried out in a few seconds. The obtained results are close to those given by marketed design tools.

The investigation of the misalignments effects on the maximum loads of the bearings using the proposed model affirms that it is imperative to consider the misalignments in the early design process phases, because it is an uncontrollable parameter and it affects considerably load distribution.

In the near future, it is planned to improve the model by the consideration of the bearing bending stiffness and of the torsional loading.

Appendix A

Matrix A:

$$\underline{A}_X: \begin{bmatrix} a_{X1} & b_{X1} & 0 & 0 & 0 \\ c_{X2} & a_{X2} & b_{X2} & 0 & 0 \\ d_X & c_{X3} & a_{X3} & b_{X3} & 0 \\ 1 & 1 & 1 & 1 & 1 \\ 0 & L_1 & L_2 & L_3 & L_4 \end{bmatrix}; \quad \underline{A}_Y: \begin{bmatrix} a_{Y1} & b_{Y1} & 0 & 0 & 0 \\ c_{Y2} & a_{Y2} & b_{Y2} & 0 & 0 \\ d_Y & c_{Y3} & a_{Y3} & b_{Y3} & 0 \\ 1 & 1 & 1 & 1 & 1 \\ 0 & L_1 & L_2 & L_3 & L_4 \end{bmatrix}$$

$$\underline{A}: \begin{bmatrix} \cos\theta[\underline{A}_X] & \sin\theta[\underline{A}_X] \\ -\sin\theta[\underline{A}_Y] & \cos\theta[\underline{A}_Y] \end{bmatrix}$$

$$L_1 = l_1; \quad L_2 = l_1 + l_2; \quad L_3 = l_1 + l_2 + l_3; \quad L_4 = l_1 + l_2 + l_3 + l_4$$

$$a_i = \frac{l_i^2}{3E J_i} + \frac{l_{i+1}^2 + 3l_i l_{i+1}}{6E J_{i+1}}; \quad b_i = \frac{l_{i+1}^2}{6E J_{i+1}}; \quad c_i = \frac{l_{i+1}(l_{i+1} + 3l_i + 3l_{i-1})}{6E J_{i+1}} + \frac{l_i(2l_i + 3l_{i-1})}{6E J_i}$$

$$d = \frac{l_3(2l_3 + 3l_1 + 3l_2)}{6E J_3} + \frac{l_4(l_4 + 3l_1 + 3l_2 + 3l_3)}{6E J_4}$$

The coefficients a_{Xi} , a_{Yi} , b_{Xi} , b_{Yi} , c_{Xi} , c_{Yi} , d_X and d_Y are obtained by replacing J_i by J_{Xi} (respectively J_{Yi}) in a_i , b_i , c_i and d .

Matrix B : $\underline{B}_X = \underline{B}_Y$:

$$\begin{bmatrix} -\frac{1}{l_1} & \frac{l_1+l_2}{l_1 l_2} & -\frac{1}{l_2} & 0 & 0 \\ 0 & -\frac{1}{l_2} & \frac{l_2+l_3}{l_2 l_3} & -\frac{1}{l_3} & 0 \\ 0 & 0 & -\frac{1}{l_3} & \frac{l_3+l_4}{l_3 l_4} & -\frac{1}{l_4} \\ 0 & 0 & 0 & 0 & 0 \\ 0 & 0 & 0 & 0 & 0 \end{bmatrix}; \quad \underline{B}: \begin{bmatrix} \cos\theta[\underline{B}_X] & \sin\theta[\underline{B}_X] \\ -\sin\theta[\underline{B}_Y] & \cos\theta[\underline{B}_Y] \end{bmatrix}$$

Matrix $\underline{\underline{C}}$:

$$\underline{\underline{C}}_X : \begin{bmatrix} e_{X1} & f_{X1} & 0 & 0 \\ g_{X2} & e_{X2} & f_{X2} & 0 \\ h_X & g_{X3} & e_{X3} & f_{X3} \\ 1 & 1 & 1 & 1 \\ M_1 & M_2 & M_3 & M_4 \end{bmatrix}; \quad \underline{\underline{C}}_Y : \begin{bmatrix} e_{Y1} & f_{Y1} & 0 & 0 \\ g_{Y2} & e_{Y2} & f_{Y2} & 0 \\ h_Y & g_{Y3} & e_{Y3} & f_{Y3} \\ 1 & 1 & 1 & 1 \\ -M_1 & -M_2 & -M_3 & -M_4 \end{bmatrix}$$

$$\underline{\underline{C}} : \begin{bmatrix} \cos\theta[\underline{\underline{C}}_X] & \sin\theta[\underline{\underline{C}}_X] \\ -\sin\theta[\underline{\underline{C}}_Y] & \cos\theta[\underline{\underline{C}}_Y] \end{bmatrix}$$

$$M_1 = 1/2l_1; \quad M_2 = l_1 + 1/2l_2; \quad M_3 = l_1 + l_2 + 1/2l_3; \quad M_4 = l_1 + l_2 + l_3 + 1/2l_4$$

$$e_i = \frac{5l_i^2}{48E J_i} + \frac{2l_{i+1}^2 + 3l_i l_{i+1}}{12E J_{i+1}}; \quad g_i = \frac{l_{i+1}(2l_{i+1} + 6l_i + 3l_{i-1})}{12E J_{i+1}} + \frac{l_i(4l_i + 3l_{i-1})}{12E J_i}; \quad f_i = \frac{l_{i+1}^2}{48E J_{i+1}}$$

$$h = \frac{l_3(4l_3 + 3l_1 + 6l_2)}{12E J_3} + \frac{l_4(2l_4 + 3l_1 + 6l_2 + 6l_3)}{12E J_4}$$

The coefficients e_{Xi} , e_{Yi} , f_{Xi} , f_{Yi} , g_{Xi} , g_{Yi} , h_X et h_Y are obtained by replacing J_i by J_{Xi} (respectively J_{Yi}) in e_i , f_i , g_i and h .

References

- [1] K. Radermacher, Das instationar belastete zylindrisches Gleitlager, Dissertation TH, Karlsruhe, Germany, 1962.
- [2] V. Gross, A.W. Hussmann, Forces in the main bearings of multicylinder engines, SAE, 1966, # 660756.
- [3] R.S. Paranjpe, S.I. Tseregounis, M.B. Viola, Comparison between theoretical calculations and oil film thickness measurements using the total capacitance method for crankshaft bearings in a firing engine, Tribol. Trans. 43 (2000) 345–356.
- [4] J.M. Conway-Jones, F.A. Martin, R. Gojon, Refinement of engine bearing design techniques, Tribol. Int. 24 (1991) 119–127.
- [5] I. Piraner, C. Pflueger, O. Bouthier, Cummings crankshaft and bearing analysis process, in: North American MDI User Conference, 2002.
- [6] F.V. Tinaut, A. Melgar, B. Gimenez, L. Fernandez, H. Huidobro, A method to determine the two components of the crankshaft load on a bearing cap in firing engines, SAE Technical Paper Series, # 2000-01-1340, 2000.
- [7] J. Sun, J. Wang, C. Gui, Whole crankshaft beam-element finite-element method for calculation crankshaft deformation and bearing load of an engine, Proc. Inst. Mech. Eng., Part J, J. Eng. Tribol. (2010) 224–299.
- [8] J.F. Booker, Dynamically loaded Journal bearings: numerical application of the mobility method, J. Lubr. Technol. – Trans. ASME, Ser. F 93 (1) (1971) 168–176.
- [9] M. Rebbert, R. Lach, P. Kley, Dynamic crankshaft stress calculation using a combination of MSS and FEA, in: International ADAMS User Meeting, 2000.
- [10] J.H. Raub, J. Jones, P. Kley, M. Rebbert, Analytical investigation of crankshaft dynamics as a virtual engine module, in: Proceedings SAE Noise and Vibrations Conference and Exposition, May 1999.
- [11] J. Sun, C.-L. Gui, J. Wang, Research on elastohydrodynamic lubrication of a crankshaft bearing with a rough surface considering crankshaft deformation, Proc. Inst. Mech. Eng., Part D, J. Automob. Eng. Mech 222 (12) (2008) 2403–2414.
- [12] B. Bellakhdhar, A. Dogui, J.-L. Ligier, Rigidité en flexion d'un vilebrequin, Méc. Ind. 12 (2011) 37–43.
- [13] B. Bellakhdhar, C. Bouraoui, A. Dogui, Analyse statique d'un arbre sur cinq appuis élastiques, désalignés et avec jeux, in: COTUME'2008, Tunisie, 2008, pp. 103–104.
- [14] Z.P. Mourelatos, A crankshaft system model for structural dynamic analysis of internal combustion engines, Comput. Struct. 79 (2001) 2009–2027.
- [15] Q. Leclere, Étude et développement de la mesure indirecte d'effort: Application à l'identification des sources internes d'un moteur diesel, thèse, Institut national des sciences appliquées de Lyon, 2003.
- [16] B. Bellakhdhar, A. Dogui, J.-L. Ligier, Main bearing stiffness investigation, Int. J. Mech. Mat. Eng. 2 (1) (2011) 8–12.
- [17] J. Frêne, Butées et paliers hydrodynamiques, Techniques de l'ingénieur n° B5 320, pp. 1–36; B5 321, pp. 1–7; B5 347, p. 1, 1995.